AUTOMATIC ANATOMY RECOGNITION VIA FUZZY OBJECT MODELS

Jayaram K. Udupa[a], Dewey Odhner[a], Alexandre X. Falcao[b], Krzysztof Chris Ciesielski[a,c], Paulo A.V. Miranda[b], Monica Matsumoto[a], George J. Grevera[a,d], Babak Saboury[e,a], Drew A. Torigian[e]

[a]Medical Image Processing Group (jay@mail.med.upenn.edu) - UPENN – Philadelphia, PA
[b]Institute of Computing – University of Campinas – Campinas, SP, Brazil
[c]Department of Mathematics – West Virginia University – Morgantown, WV
[d]Department of Mathematics and Computer Science – Saint Joseph's University – Philadelphia, PA
[e]Department of Radiology – Hospital of the University of Pennsylvania – Philadelphia, PA

ABSTRACT

To make Quantitative Radiology a reality in routine radiological practice, computerized automatic anatomy recognition (*AAR*) during radiological image reading becomes essential. As part of this larger goal, last year at this conference we presented a fuzzy strategy for building body-wide group-wise anatomic models. In the present paper, we describe the further advances made in fuzzy modeling and the algorithms and results achieved for *AAR* by using the fuzzy models. The proposed *AAR* approach consists of three distinct steps: (a) Building fuzzy object models (*FOMs*) for each population group *G*. (b) By using the *FOMs* to recognize the individual objects in any given patient image *I* under group *G*. (c) To delineate the recognized objects in *I*. This paper will focus mostly on (b).

FOMs are built hierarchically, the smaller sub-objects forming the offspring of larger parent objects. The hierarchical pose relationships from the parent to offspring are codified in the *FOMs*. Several approaches are being explored currently, grouped under two strategies, both being hierarchical: (*ra*1) those using search strategies; (*ra*2) those strategizing a one-shot approach by which the model pose is directly estimated without searching. Based on 32 patient CT data sets each from the thorax and abdomen and 25 objects modeled, our analysis indicates that objects do not all scale uniformly with patient size. Even the simplest among the (*ra*2) strategies of recognizing the root object and then placing all other descendants as per the learned parent-to-offspring pose relationship bring the models on an average within about 18 *mm* of the true locations.

Keywords: Shape Modeling, Fuzzy Sets, Object Recognition, Segmentation, Fuzzy Connectedness, Fuzzy Models

1. INTRODUCTION

Since the birth of radiology in 1895, the emphasis in clinical radiology has been on *human visualization* of internal structures. Since radiography could not unravel internal information in an un-obscured manner, the continued quest for internal body visualization heralded various tomographic image modalities for deriving anatomic, functional, and molecular information. However, this emphasis on human visualization continued and the practice of *clinical radiology* has remained mostly *qualitative*, *descriptive* and *subjective*. Quantification is amply employed in radiology in clinical research. However, in clinical radiological practice, this is rare. In this qualitative mode, quantifiable and/or subtle image information is underutilized, interpretations remain subjective, and subtle changes due to early disease or therapeutic intervention may be underestimated or missed [1]. It is widely recognized that if *Quantitative Radiology* (*QR*) can be brought to routine clinical practice, numerous advances can be made ranging from: improved sensitivity, specificity, accuracy, and precision of early disease diagnosis; more objective and *standardized* response assessment of diseases to treatment; improved understanding of what is "normal"; increased ease of disease measurement and reporting; discovery of new disease biomarkers; better outcome assessment; effective handling of the large volume of image information; and effective combined utilization of multimodality image information.

Medical Imaging 2012: Image-Guided Procedures, Robotic Interventions, and Modeling,
edited by David R. Holmes III, Kenneth H. Wong, Proc. of SPIE Vol. 8316, 831605

We envision a *QR* system to operate in the clinic in the following manner. Imagine we build a family of body-wide models, at a desired resolution of the population variables (gender, age, etc.), complete with anatomic, organ geographic, dynamic, physiological, and functional information. Supported by the model family, the implemented *QR* system will then automatically recognize and delineate the anatomy in the given patient image(s) during clinical image interpretation, highlight deviations from normality, and list a host of pertinent quantitative measures, indicating their normal range for the particular group to which the patient belongs, highlighting out-of-range measures if any.

To make *QR* a reality in routine clinical radiological practice, computerized *Automatic Anatomy Recognition* (*AAR*) during radiological image reading becomes essential. The goal of *AAR* is: given a patient image set for a specific body region, to identify and delineate the various organs in the body region automatically. Given the clinical image reading setting, with potentially lower quality images and the need for greater degree of automation than in research settings, the methodology devised for a *QR* system should take an approach that is as much as possible general and independent of the organs, body region, imaging modality, and the imaging protocols. Given the difficulties in image segmentation and the vagaries of clinical imaging scenarios, it is imperative that body-wide models representing normal populations be created to serve in *AAR*.

The novelty in our effort stems from the following three considerations. First, most of the anatomy modeling methods to date has focused on specific organs or organ systems and not on the multitude of organs body-wide. This difference evokes its own challenges. Second, except for our own earlier work [2-4], the reported modeling strategies all have a statistical theoretical framework, in the form of statistical shape modeling [5], statistical atlases [6], *etc*. Probabilistic and fuzzy techniques have been co-developed in many endeavors including image analysis and segmentation. They start off with different axioms, use different mathematical constructs, and lead to very different algorithms in imaging. Our motivation for pursuing the development of fuzzy anatomy modeling principles is to find natural and computationally efficient means of bringing anatomic knowledge about large assemblies of objects into graph-based approaches such as fuzzy connectedness [7]. This allows us to pursue an all-digital fuzzy approach without seeking continuous approximations or making crucial assumptions on random phenomena and their distributions, etc. Third, we model the hierarchical arrangement inherent in the anatomic layout of organs and exploit this codification to make *AAR* effective and efficient. There are several components to the *AAR*-*QR* project we are pursuing: (C1) gathering body-wide group-wise image data for *normal* subjects; (C2) building fuzzy models and evaluating them; (C3) using fuzzy models to recognize and delineate anatomy in a given patient image set; (C4) detecting and delineating pathology; (C5) quantification; (C6) computational set up for interactive-rate performance. In this paper our focus will be on (C3), specifically on recognizing anatomic organs in the torso. About 25 organs in the thoracic, upper and lower abdominal, and pelvic region are considered.

2. FUZZY MODELS

This section summarizes the fuzzy modeling approach. For details see [4].

We will use the following notation. We will think of the *whole body*, *WB*, as being divided into *body regions*, $B_1,\ldots,B_r$, for example, head, neck, thorax, abdomen, pelvis, etc. We will denote an image acquired for a body region B by $I = \langle C, f \rangle$ where $C \subset Z^3$ is the domain of I covering B, and f: $C \rightarrow R$ is the image intensity function. The elements of C will be called voxels and the values $f(v)$ assigned to $v \in C$ will be referred to as the intensity of v in I. Our idea is to build models that represent normalcy. Our approach to model building relies on patient images, available in our hospital image database, that are certifiably normal for specific body regions. This is a more practical and less expensive strategy than requiring prospective image acquisition expressly for the purpose of building models. On the flip side, clinical images are acquired rarely for the whole body but typically only for specific body regions. This necessitates our approach of building models by body region to eventually assemble these models properly to create the model for *WB*. Most of our description below therefore pertains to a (any) body region B.

Models are built for each subject group, G, separately. Each group G is defined at a desired resolution of the population variables such as age, gender, race, etc. Let $I_1,\ldots,I_N$ be the images of B acquired from N subjects, all belonging to a particular group G and let $O_1,\ldots,O_L$ be the organs in B considered for modeling. The fuzzy organ model of B, $FOM(B)$, is then considered to be a quintuple $FOM(B) = \langle H, M, \rho, \lambda, \eta \rangle$.

H here, represented as a tree, is the hierarchical order considered in the model for the organs and sub-organs in B. The hierarchy represents the natural anatomic order of the organs in B or an order that is motivated by the effectiveness of

object recognition. Our efforts have so far focused on the thoracic and abdominal body regions. The hierarchies of organs employed for these regions are depicted in Figs. 1(a) and (b).

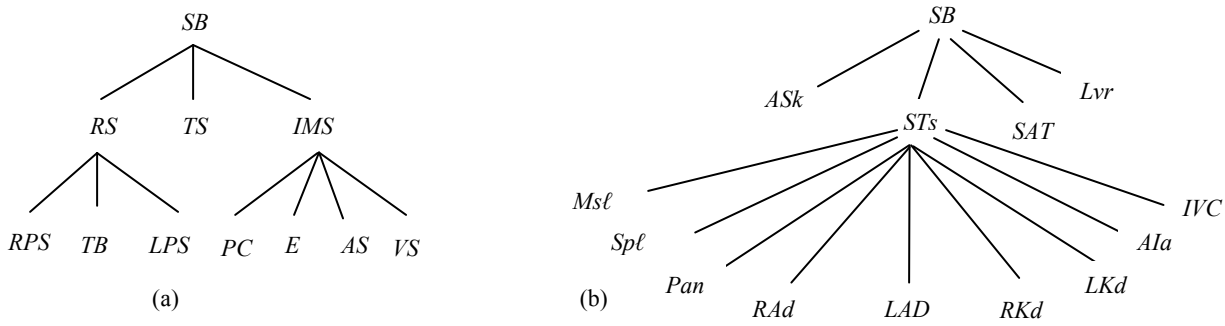

Figure 1: The hierarchy of the organs considered for modeling. (a) B = thorax. *SB*: Skin Boundary; *RS*: Respiratory System; *TS*: Thoracic Skeleton; *IMS*: Internal Mediastinum; *RPS* & *LPS*: Right & Left Plural Space; *TB*: Trachea & Bronchi; *PC*: Pericardium; *AS* & *VS*: Arterial & Venous System. (b) B = Abdomen. *SB*: Skin boundary; *ASk*: Abdominal Skeleton; *STs*: Soft Tissue; *SAT*: Subcutaneous Adipose Tissue; *LVr*: Liver; *MSℓ*: Muscle; *SPℓ*: Spleen; *Pan*: Pancreas; *RAd* & *LAd*: Right & Left Adrenal Gland; *RKd & LKd:* Right & Left Kidney; *AIa*: Aorta & Iliac Arteries; *IVC*: Inferior Vena Cava & Iliac Veins.

The second item M is a family of fuzzy models, one fuzzy model FM_ℓ associated with each organ O_ℓ, $M = \{FM_\ell: 1 \leq \ell \leq L\}$. FM_ℓ models how organ O_ℓ varies within its population of N samples. It is represented as a fuzzy subset of the body region, with a membership value $\mu_\ell(v)$ assigned to each geographically located voxel v. This value is estimated by propagating each organ shape inwardly and outwardly from the boundary and by determining how these propagated shapes from the population meet at v.

The third item, $\rho = \{\rho_{\ell,k}: O_\ell$ is a parent of O_k in H, $1 \leq \ell, k \leq L\}$, describes the position and orientation relationships, and their variation, between each offspring object O_k and its parent O_ℓ in the hierarchy. For the root object, which has no parent, $\rho_{\ell,k}$ is assumed to be its relationship to the scanner coordinate system.

The fourth item, λ, is a family $\{\lambda_\ell: 1 \leq \ell, k \leq L\}$, where each λ_ℓ expresses the variation in scale factor (size) of organ O_ℓ over its population.

The last item, η, represents the statistics of a set of measurements pertaining to the organ assembly in B.

The concepts underlying $FOM(B)$ can be readily extended from body region B to the whole body WB. The hierarchy now will have the WB region at its root and $B_1,\ldots,B_r$ as the immediate descendants. The node corresponding to each body region B will then have a sub-tree, rooted at that node, which represents the hierarchy associated with B. We hope to build a body-wide model $FOM(WB)$ eventually by the piece-meal approach of building models for each body region B separately. In the rest of this paper, our focus will be on AAR as applicable to a given body region B.

3. ANATOMY RECOGNITION

Once a model $FOM(B)$ is built for a body region B and a population group G, our task is to perform AAR in a given image I of the body region B of a patient who belongs to group G. We think of the AAR task to consist of two components: *recognition* and *delineation*. The goal of recognition is to determine *where* organs $O_1,\ldots,O_L$ are in I, meaning, to determine the best *pose* (location, orientation, and scale factor) for the models $FM_1,\ldots,FM_L$ at which they are to be placed in I so they fall in place as closely as possible to the actual organ manifestation in I. The goal of delineation is to *mark* the precise spatial occupation of $O_1,\ldots,O_L$ in I. Although the two components are interdependent and operate in tandem, this paper's focus will be only on recognition.

Our approach to AAR, specifically to recognition, is hierarchical. First the root object is recognized in I. Then the descendants O_k are recognized from a knowledge of the pose of their already recognized parent O_ℓ and the parent-to-offspring relationship $\rho_{\ell,k}$ as well as evidence garnered from I. The AAR recognition procedure is as follows.

Procedure *AAR-R*

In: An image I of B and $FOM(B)$, both for group G.

Out: Poses for FM_ℓ, $1 \le \ell \le L$, in I.

Begin

*R*1. Call recognition algorithm $RA_0(O)$ to determine the pose of the root object O in I.

*R*2. *Repeat*

*R*3. Traverse down H and determine the offspring object O_k to be recognized next.

*R*4. Knowing the pose of the parent object O_ℓ, relationship $\rho_{\ell,k}$, and scale range λ_k, call $RA(O_k)$ to determine the pose of O_k in I.

*R*5. *Until* all objects are covered in H.

*R*6. Output poses in I for all objects.

End

For an effective *AAR* system, recognition and delineation need to be coupled synergistically. This can improve the effectiveness of both recognition and delineation [8]. In fact, a call for a delineation algorithm will have to be interspersed in the above procedure (for example, between *R*1 and *R*2 and between *R*4 and *R*5), and recognition and delineation may have to be iterated alternately to fully express the synergy existing between them. Since the focus here is on recognition, we will leave out such matters from this paper.

We have been experimenting with several strategies for the recognition algorithm RA_0 and RA. These may be grouped into two categories – (*ra*1): those using search strategies to seek the "best" pose for the models in I; (*ra*2): those strategizing a one-shot approach by which the model pose in I is directly estimated without searching. We have implemented and tested the following three methods under these strategies – Methods 1 and 2 under *ra*1 and Method 3 under *ra*2.

In all search approaches (*ra*1), we have ignored the angular orientation and considered only the object center location and the scale factor. That is, the search space is 4-dimensional. To determine the optimum pose for object O_k, a subset of this 4D space is determined based on the variations observed in $\rho_{\ell,k}$ and λ_k. This subspace is then sampled at regular discrete intervals, and at each sample pose, a "recognition score" is valuated to examine the degree of match of FM_k with the intensity patterns in I. The pose returning the maximum score is considered to be the pose recognizing object O_k.

Method 1: Using Fisher Linear Discriminant (*FLD*)

FLD [9] is a non-parametric pattern classification technique which we employ here in a supervised learning mode. In the learning phase, during model building, for each organ O_k, a linear discriminant (a separating line in the feature space) that optimally separates the image-derived features of O_k from the image-derived features of the background of O_k is determined as described below. In the recognition phase, this discriminant is used to determine the optimum pose of O_k.

We employ three features f_1, f_2, and f_3 to characterize the appearance of the boundary of organ O_k as well as its background in the training images $I_1,\ldots,I_N$. Consider a pixel edge e described by $e = \{c, d\}$ where c and d are 4-adjacent pixels in a slice of any of these images $J = \langle C, f \rangle$. To every edge e, we assign the features f_1, f_2, and f_3 in the following manner: $f_1 = min\{f(c), f(d)\}$, $f_2 = max\{f(c), f(d)\}$, and f_3 is the signed gradient magnitude of f evaluated at e. The sign is positive if the gradient direction is in agreement with the direction of increasing signed distance from the boundary (counting distance inside the object as negative and outside as positive) of O_k in J.

For the purposes of *FLD* design, the "object" class for O_k is represented by the set of features $S_k = \{(f_1, f_2, f_3)^t$: e is a pixel edge "near" the boundary of O_k in any of $I_1,\ldots,I_L\}$. Similarly the "background" class of O_k is defined by $B_k = \{(f_1, f_2, f_3)^t$: e is a pixel edge "away" from the boundary of O_k in any of $I_1,\ldots,I_L\}$. A linear discriminant that optimally separates S_k and B_k for each organ O_k is determined via the *FLD* method [9].

In the recognition phase, for each searched pose $\boldsymbol{p}$ of FM_k in I, a recognition score $F_{\boldsymbol{u}}(\boldsymbol{p})$ is determined as follows. Let $\boldsymbol{u}$ be the vector normal to the best separating *FLD* plane found at training. Let $Bd(FM_k) = \{(c, d)$: c and d are 6-adjacent &

$\mu_k(c) \geq 0.5$ & $\mu_k(d) < 0.5\}$, where μ_k is the membership function of FM_k, be a hard boundary surface derived from FM_k, by thresholding FM_k at 0.5. Let S_k' be the set of feature vectors sampled on $Bd(FM_k)$ at pose $\boldsymbol{p}$. The recognition score is then taken to be $F_{\boldsymbol{u}}(\boldsymbol{p}) = (\sum_{\boldsymbol{v} \in S_k'} \boldsymbol{v}) \bullet \boldsymbol{u}$. The pose that yields the maximum value for $F_{\boldsymbol{u}}(\boldsymbol{p})$ is taken to be the recognized pose.

Method 2: Minimizing ball-scale-based energy

In this method, an optimum pose for FM_k in I is determined by minimizing an energy function that is formulated by using the concept of ball scale (*b*-scale) [10]. The idea behind *b*-scale is to treat the basic elements of an image (such as *I*) not as voxels but as balls of uniform intensity. For $I = \langle C, f \rangle$, its b-scale image $I_b = \langle C, f_b \rangle$ is such that, for any $c \in C$, $f_b(c)$ is the radius of the largest ball centered at c within which f is "homogeneous". The energy function associated with FM_k at pose $\boldsymbol{p}$ in I is $E(\boldsymbol{p}) = \sum_{c \in Q_{\boldsymbol{p}}} f_b(c)$.

Method 3: One-shot recognition

In this strategy, the root object is first recognized in I by the method described below. All other objects are then subsequently positioned in I based on the found root object pose and the mean $\rho_{\ell,k}$ from the model. The objects are also scaled by the scale factor found for the root object.

To recognize the root object *SB*, a threshold is applied to I to roughly separate the foreground voxels, and a morphological opening operation is performed to remove extraneous material such as the scanner table. The position of the model of *SB* in I is determined to be the geometric center of this roughly segmented object. Its scale factor is estimated from its linear size measure, which, in this paper is taken to be the square root of the principal eigenvalue resulting from a principal component analysis of the binary object. (We have examined the use of other size measures in model building such as the length of the diagonal of a box that just encloses O_ℓ and the cube root of the volume of O_ℓ [4].)

4. EXPERIMENTAL ANALYSIS

Image data: In this paper we present results for the Thorax and Abdomen. Institutional Review Board approval for this study was obtained prior to study initiation. Subsequently, from our hospital image database, we have gathered contrast-enhanced breath-hold CT images taken from 32 male subjects of age range 50-60 years for the thoracic and abdominal body regions separately. The board certified radiologist participating in this project (DAT) examined all image data and certified them to be radiologically normal for the body region for which they are considered. Since the data are from routine clinical scans, they are of clinical spatial resolution, with a typical voxel size of $0.9mm \times 0.9mm \times 5mm$.

Fuzzy Models: For each body region, we have randomly divided the 32 data sets into a training set (of 16), used for model building, and a testing set (of 16) for evaluating recognition performance. We have included 11 and 14 organs in the two body regions as depicted in Fig. 1. Fig. 2 displays the rendered surfaces of some of these organs taken from one of the training data sets. Models are built separately for the two body regions. Fig. 3 depicts some of the fuzzy models in different combinations of the organs for the two body regions, shown as volume renditions. Given the 16 segmented data sets for the L organs (= 11 and 14 for the Thorax and Abdomen), the model building step takes a total computational time of respectively 86 *min* and 225 *min* on an Intel Pentium 4 platform with a 3.6 GHz CPU and 3 GB RAM.

AAR: Fig. 4 displays some recognition results for each of the three methods (in each row) wherein a slice of a test image I is shown together with, as an overlay, the corresponding cross section of FM_ℓ at the best pose determined by the recognition method. The mean computational time for recognizing all objects per patient is: Method 1 – 25 *min* 42 *s*, Method 2 – 23 *min* 37 *s*. Method 3 – 1 *min* 12 *s*.

Since all (32 + 32) data sets have been previously segmented manually and verified (by DAT and SB) for accuracy and used for testing different scenarios of model building, they can be used for testing the accuracy of the recognition techniques as well. In this initial effort, we have ignored organ orientation information in both the model building process and estimating the recognition pose. (Actually our tests indicate that considering orientation at model building (alone) has little influence on recognition results.) Therefore, we will express recognition accuracy in terms of location and scale factor. Location error will be expressed in terms of the distance between the geometric centers of O_ℓ in the

reference segmentation and FM_ℓ at the recognized pose (ideally this distance should be 0). Scale factor discrepancy will be described as a ratio of the true size to the estimated size (ideally 1). Tables 1 and 2 list the mean location and scale factor errors and their standard deviation over the 16 tested data sets for all organs for the Thorax and Abdomen.

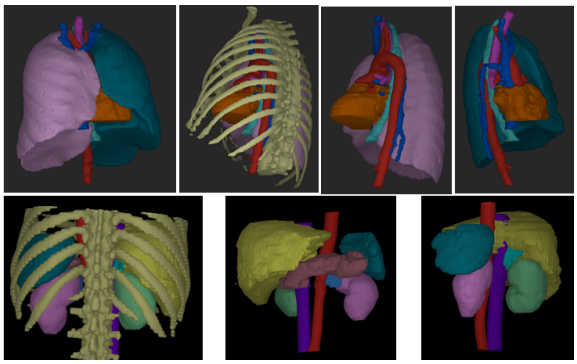

Fig. 2: 3D renditions of some of the sample objects for which fuzzy models are built.

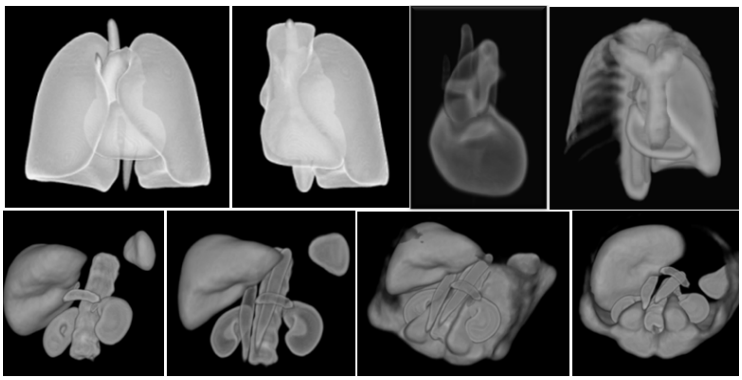

Fig. 3: Volume renditions of some of the fuzzy models FM_ℓ built for the organs in the Thorax (top row) and Abdomen (bottom row).

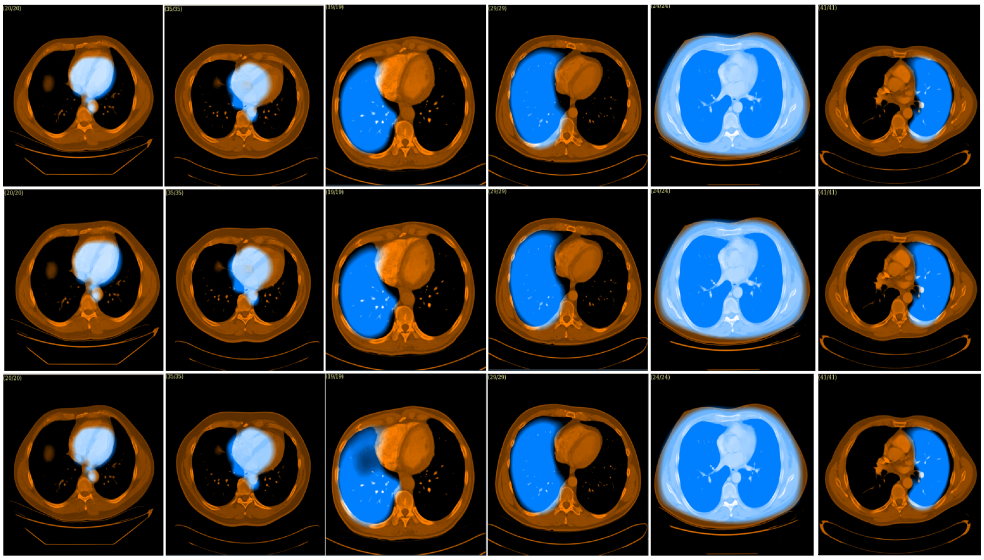

Fig 4: Slice displays of some recognition results for the *FLD* (top row), *b*-scale (middle row), and one-shot (bottom row) methods for the Thorax data. The cross sections of the fuzzy models at the recognition pose are shown overlaid on the image slices. The objects for which the models are displayed are: IMS, RPS, SB, and LPS.

Method		*LPS*	*IMS*	*RPS*	*SB*	*RS*	*TS*	*AS*	*VS*	*E*	*TB*	*PC*
FLD	Location (*mm*)	20.4 (7.7)	21.7 (15.6)	32.8 (13.9)	4.8 (2.1)	17.5 (7.8)	12.8 (7.0)	15.4 (5.9)	25.4 (15.5)	18.4 (11.2)	12.3 (9.0)	28.0 (13.5)
	Scale	0.98 (0.09)	1.04 (0.1)	1.04 (0.08)	1.03 (0.03)	1.0 (0.04)	1.03 (0.09)	1.09 (0.13)	1.05 (0.15)	1.02 (0.12)	0.97 (0.17)	0.94 (0.09)
***b*-scale**	Location (*mm*)	18.4 (6.9)	18.1 (15.6)	28.4 (12.0)	4.6 (1.8)	20.0 (8.1)	12.3 (6.5)	12.8 (6.3)	20.2 (14.6)	16.1 (10.4)	17.6 (10.5)	34.1 (12.1)
	Scale	1.03 (0.09)	1.06 (0.11)	1.04 (0.09)	1.03 (0.03)	1.02 (0.02)	1.03 (0.09)	1.14 (0.15)	1.08 (0.17)	1.02 (0.13)	1.01 (0.15)	1.05 (0.1)
One-shot	Location (*mm*)	20.1 (8.1)	21.7 (14.8)	28.5 (14.4)	3.5 (1.6)	22.6 (12.9)	11.6 (7.0)	15.9 (6.3)	23.5 (15.0)	19.1 (12.5)	21.5 (12.0)	31.6 (14.2)
	Scale	1.05 (0.09)	1.08 (0.1)	1.06 (0.09)	1.06 (0.02)	1.05 (0.09)	1.06 (0.06)	1.14 (0.15)	1.1 (0.16)	1.05 (0.11)	1.03 (0.13)	1.06 (0.1)

Table 1: Recognition accuracy for the organs of the Thorax. Standard deviation is in parenthesis.

Method		*SB*	*ASk*	*STs*	*SAT*	*Lvr*	*Msℓ*	*Spℓ*	*Pan*	*AIa*
One-shot	Location (*mm*)	5.2 (2.1)	26.3 (11)	12.9 (3.1)	17.5 (10.7)	27.7 (12.9)	11.4 (4.7)	25.5 (8.8)	19.7 (5.9)	26.5 (8.9)
	Scale	1.02 (0.03)	1.0 (0.06)	1.0 (0.04)	1.01 (0.03)	0.99 (0.09)	1.0 (0.03)	1.02 (0.14)	0.91 (0.14)	1.05 (0.15)

Table 2: Recognition accuracy for some of the tested organs of the Abdomen. Standard deviation is in parenthesis.

5. REMARKS

Overall the *b*-scale method seems to perform better than the *FLD* and one-shot methods. There is no statistically significant difference between *FLD* and b-scale methods ($p = 0.227$). There is however statistical difference between the b-scale and one-shot methods ($p << 0.05$) and the FLD and one-shot methods ($p = 0.059$). The computational advantage of the one-shot method weighs in its favor to make it overall the best strategy among these three methods.

Note that the estimation of scale factor is overall excellent. The estimation of location is within 20*mm* (actually overall mean = 18.4*mm* for the Thorax) of the true location for most of the objects. In our previous work with hybrid graph-based delineation algorithms combined with models [8, 11], we have observed that if the model can be brought within 25 pixels of the true location, then those algorithms yield a delineation accuracy of 95% or better for true positive volume and 5% or less for false positive volume. The overall mean location error in our experiments is about 20 pixels. Although we have not yet carried out detailed studies on final organ delineation in this work, the recognition accuracy we have achieved seems to bode well for the delineation accuracy that can be achieved.

RPS and *PC* seem to fare poorer than the rest of the organs. We believe this stems from the fact that there is considerable variation in the position of *RPS* and *PC* relative to their parent organs in different subjects. For *PC*, this is due to the motion of the heart, and for *RPS*, it is due to the liver pressing against the diaphragm and thus changing the shape of *RPS* differently in different subjects. Also there may be differences in the respiratory phase of the breath-hold instant at which images are acquired from the different subjects.

Our future efforts will be to bring textural information into the one-shot recognition process, to complete the whole *AAR* process including delineation, to speed up the computational processes, and to start deploying the *AAR* system in *QR* applications.

ACKNOWLEDGEMENTS

This work is partially supported by a DHHS grant HL105212.

REFEFENCES

[1] Torigian, D.A. and Alavi, A.: "The evolving role of structural and functional imaging in assessment of age-related changes in the body," *Seminars in Nuclear Medicine*, 37:64-68 (2007).

[2] Miranda, P.A.V., Falcao, A.X., and Udupa, J.K.:"Clouds: A model for synergistic image segmentation," *Proceedings of the ISBI*, pp 209-212, Paris, France, May 14-17, (2008).

[3] Miranda, P.A.V., Falcao, A.X. and Udupa, J.K.: "Cloud Bank: A multiple clouds model and its use in *MR* brain image segmentation." *The Sixth IEEE International Symposium on Biomedical Imaging: From Nano to Macro* (ISBI), Boston MA, ISBN 978-1-4244-3932-4/09, doi: 10.1109/ISBI. 2009, 5193095, *IEEE*, June 28th – July 1st, pp. 506-509, (2009).

[4] Udupa, J.K., Odhner, D., Falcao, A.X., Ciesielski, K.C., Miranda, P.A.V., Vaideeswaran, P., Mishra, S., Grevera, G.J., Saboury, B., Torigian, D.A.: "Fuzzy object modeling," *Medical Imaging* 2011: *Proceedings of SPIE* 7964:79640B-1-10, 2011.

[5] Deserno, T.M. (editor): *Recent Advances in Biomedical Image Processing and Analysis*, Springer: Heidelberg, Germany, 2011.

[6] Lotjonen, J.M.P., Wolz, R., Koikkalainen, J.R., Thurfjell, L., Waldemar, G., Soininen, H., Rueckert, D.: "Fast and robust multi-atlas segmentation of brain magnetic resonance images," *Neuroimaging,* 49:2352-2365, 2010.

[7] Ciesielski, K.C., Udupa, J.K., Falcao, A.X., Miranda, P.A.V.: "Comparison of fuzzy connectedness and graph cut segmentation algorithms," *Medical Imaging* 2011: *Proceedings of SPIE*, 7962:796203-1-13, 2011.

[8] Liu, L. and Udupa, J.K.: "Oriented active shape models," *IEEE Transactions on Medical Imaging*, 28(4):571-584, 2009.

[9] Duda, R.O., Hart, P.E., Stork, D.G.: *Pattern Classification*, 2nd Edition, Wiley Interscience: New York, NY, 2001.

[10] Saha, P. and Udupa, J.K.: "Scale-based fuzzy connected image segmentation: Theory, algorithms and validation," *Computer Vision and Image Understanding*, 77(2):145-174, 2000.

[11] Chen, X., Udupa, J.K., Alavi, A., Torigian, D.A.: "Automatic anatomy recognition via multiobject oriented active shape models," *Medical Physics*, 37(12):6391-6401, 2010.